

# First-principles investigation of finite-temperature behavior in small sodium clusters

Mal-Soon Lee,<sup>a)</sup> S. Chacko,<sup>b)</sup> and D. G. Kanhere<sup>c)</sup>

Centre for Modeling and Simulation and Department of Physics, University of Pune,  
Ganeshkhind, Pune-411 007, India

(Received 5 July 2005; accepted 29 August 2005; published online 26 October 2005)

A systematic and detailed investigation of the finite-temperature behavior of small sodium clusters,  $\text{Na}_n$ , in the size range of  $n=8-50$  are carried out. The simulations are performed using density-functional molecular dynamics with ultrasoft pseudopotentials. A number of thermodynamic indicators such as specific heat, caloric curve, root-mean-square bond-length fluctuation, deviation energy, etc., are calculated for each of the clusters. Size dependence of these indicators reveals several interesting features. The smallest clusters with  $n=8$  and 10 do not show any signature of melting transition. With the increase in size, broad peak in the specific heat is developed, which alternately for larger clusters evolves into a sharper one, indicating a solidlike to liquidlike transition. The melting temperatures show an irregular pattern similar to the experimentally observed one for larger clusters [Schmidt *et al.*, *Nature (London)* **393**, 238 (1998)]. The present calculations also reveal a remarkable size-sensitive effect in the size range of  $n=40-55$ . While  $\text{Na}_{40}$  and  $\text{Na}_{55}$  show well-developed peaks in the specific-heat curve,  $\text{Na}_{50}$  cluster exhibits a rather broad peak, indicating a poorly defined melting transition. Such a feature has been experimentally observed for gallium and aluminum clusters [Breux *et al.*, *J. Am. Chem. Soc.* **126**, 8628 (2004); Breux *et al.*, *Phys. Rev. Lett.* **94**, 173401 (2005)]. © 2005 American Institute of Physics. [DOI: 10.1063/1.2076607]

## I. INTRODUCTION

Finite-temperature studies of finite-sized systems have been a topic of considerable interest during the last decades. Recent experimental as well as theoretical studies have brought out a number of intriguing results. In a series of experiments on free sodium clusters in the size range of 55–350, Haberland and co-workers<sup>1</sup> have observed a large size-dependent fluctuation in the melting temperatures. They have also observed a substantial lowering of about 30% in the melting temperatures as compared to that of the bulk. Interestingly, recent experiments by Jarrold and co-workers<sup>2,3</sup> show that small clusters of Sn and Ga have higher-than-bulk melting temperatures. In our previous investigations, we have attributed this higher-than-bulk melting temperatures mainly to the covalent bonding in these clusters, as against metallic bonding in the bulk phase.<sup>4,5</sup> Very recently Breux *et al.* have seen a remarkable size-sensitive feature of the melting transition of gallium as well as aluminum clusters.<sup>6,7</sup> Their experiments show that the nature of the heat-capacity curve changes dramatically with the addition of few atoms. For instance,  $\text{Ga}_{30}^+$  does not show an obvious melting transition, while  $\text{Ga}_{31}^+$  exhibit a well-defined peak, and  $\text{Ga}_{32}^+$  shows a broad peak in the heat capacity.

A number of computer simulations on the melting of small sodium clusters have been reported in literature. Calvo and Spiegelmann<sup>8</sup> have performed extensive simulations on

Na clusters in the size range of 8–147. Their simulations employed the second moment approximation (SMA) potential of Li *et al.*<sup>9</sup> as well as the distance-dependent tight-binding (DDTB or TB) method. They found more than one peak in the heat capacity of most of the clusters studied. They further observed that the nature of the ground-state geometry is crucial to precisely understand the thermodynamic properties of clusters. However, although the method they employed provide relatively good statistics required to converge the features in the caloric curve, it did not incorporate the essential ingredients of electronic structure effects. These simulations hence failed to reproduce the crucial features of the experimental results, clearly bringing out the importance of incorporating the electronic structure effects. In a very recent study,<sup>10</sup> we have successfully reproduced the melting temperatures of  $\text{Na}_N$  ( $N=55, 92, 142$ ) using the Kohn-Sham- (KS) based approach<sup>11</sup> of the density-functional theory (DFT) and also gave a plausible explanation on its irregular variation. There have also been a few theoretical investigations on the melting of sodium clusters with sizes  $n < 55$ . Rytönen *et al.*<sup>12</sup> have investigated the melting transition of  $\text{Na}_{40}$  cluster using *ab initio* method. They raised the temperature of the system from 150 to 400 K at the rate of 5 K/ps, and found that the melting transition occurs at the temperatures between 300 and 350 K. They also show that  $\text{Na}_8$  exhibits only isomerization. Aguado *et al.*<sup>13</sup> have performed Car-Parrinello orbital-free simulations to investigate the melting phenomena in  $\text{Na}_8$  and  $\text{Na}_{20}$ . Their simulation times were 8–60 ps/temperature. They observed a clear peak for  $\text{Na}_8$  and double peaks for  $\text{Na}_{20}$  in the specific-heat curve.

<sup>a)</sup>Electronic mail: mslee@unipune.ernet.in

<sup>b)</sup>Electronic mail: chacko@unipune.ernet.in

<sup>c)</sup>Electronic mail: kanhere@unipune.ernet.in

We have also investigated the melting transition in these clusters using various methods, and found a model dependence in the melting characteristics.<sup>14</sup>

In the present work, we perform density-functional molecular-dynamics simulations on  $\text{Na}_n$  clusters ( $n=8, 10, 13, 15, 20, 25, 40,$  and  $50$ ) to investigate their thermodynamic properties, specifically the size-dependent features. We perform simulations with about 150 ps/temperature which is much larger simulation times than any other earlier work. In addition to the standard indicators such as specific heat, caloric curve, and root-mean-square bond-length fluctuations, we also calculate the energy deviation, the potential-energy difference between the solidlike state and the liquidlike state, etc.

In Sec. II, we describe the computational details, followed by the results and discussion in Sec. III. Finally, we summarize the results in Sec. IV.

## II. COMPUTATIONAL DETAILS

We carry isokinetic Born-Oppenheimer molecular-dynamics calculations<sup>15</sup> using Vanderbilt's ultrasoft pseudopotentials<sup>16</sup> within the local-density approximation (LDA), as implemented in the VASP package.<sup>17</sup> We use two different methods to obtain the ground-state and several equilibrium geometries for each of the clusters. First, a "basin hopping" algorithm<sup>18</sup> is employed to generate few tens of structures for smaller clusters and several hundreds structures for larger clusters using the SMA parametrized potential of Li *et al.*<sup>9</sup> Several of these geometries, say, the lowest 10–70 geometries, are then optimized using the *ab initio* density-functional method.<sup>19</sup> In the second method, we obtained few more equilibrium geometries by optimizing several structures selected from high-temperature *ab initio* molecular-dynamics runs, typically taken from temperatures near and well above the melting temperatures of the clusters. The simulations have been carried out for 12 temperatures in the range of  $100 \text{ K} \leq T \leq 750 \text{ K}$  for  $n=8$  and 10, 9–12 temperatures in the range of  $100 \text{ K} \leq T \leq 450 \text{ K}$  for the rest of the clusters. For all the cases, the simulation time is 150 ps/temperature. We have discarded the first 30 ps for each temperature to allow for thermalization. An energy cut-off of 3.6 Ry (Refs. 20 and 21) is used for the plane-wave expansion of the wave function, with a convergence in the total energy of the order of  $10^{-4}$  eV. The resulting ionic trajectory data have been used to study the melting of clusters by analyzing various thermodynamic indicators, which are discussed below in detail.

We calculate the deformation parameter,  $\varepsilon_{\text{def}}$ , to analyze the shape of the ground-state geometry for all the clusters. The shape of the ground-state geometry plays a crucial role in determining the thermodynamic properties of a cluster. The deformation parameter,  $\varepsilon_{\text{def}}$ , is defined as

$$\varepsilon_{\text{def}} = \frac{2Q_1}{Q_2 + Q_3},$$

where  $Q_1 \geq Q_2 \geq Q_3$  are eigenvalues of the quadrupole tensor  $Q_{ij} = \sum_I R_{iI} R_{jI}$  with  $R_{iI}$  being the  $i$ th coordinate of ion  $I$  relative to the center of mass of the cluster. A spherical system

( $Q_1 = Q_2 = Q_3$ ) has  $\varepsilon_{\text{def}} = 1$ , while  $\varepsilon_{\text{def}} > 1$  indicates a quadrupole deformation of some kind.

To analyze the thermodynamic properties, we first calculate the ionic specific heat and the average potential energy per temperature (the caloric curve). We extract the classical ionic density of states,  $\Omega(E)$ , of the system, or equivalently the classical ionic entropy,  $S(E) = \kappa_B \ln \Omega(E)$ , via the multiple histogram method<sup>22</sup> to evaluate the canonical specific heat. In the canonical ensemble, the specific heat is defined as  $C(T) = \partial U(T) / \partial T$ , where  $U(T) = \int E p(E, T) dE$  is the average total energy. The probability of observing an energy  $E$  at a temperature  $T$  is given by the Gibbs distribution  $p(E, T) = \Omega(E) \exp(-E / \kappa_B T) / Z(T)$ , with  $Z(T)$  the normalizing canonical partition function. We normalize the calculated canonical specific heat by the zero-temperature classical limit of the rotational plus vibrational specific heat, i.e.,  $C_0 = (3N - 9/2) \kappa_B$ . Details of this method can be found in Ref. 14. The melting temperature has been taken as a peak in the specific-heat curve, following the convention of the experiments.<sup>1</sup>

The other thermodynamic indicator calculated is the root-mean-square bond-length fluctuations (RMSBLF), i.e., the Lindemann-type criterion for a finite system, given as

$$\delta_{\text{rms}} = \frac{2}{N(N-1)} \sum_{i < j} \frac{\sqrt{\langle R_{ij}^2 \rangle_t - \langle R_{ij} \rangle_t^2}}{\langle R_{ij} \rangle_t},$$

where  $R_{ij}$  is the distance between the  $i$ th and  $j$ th ions. This quantity gives the average fluctuation in the average bond lengths that are occurring at a given temperature. A value of about 0.1–0.15 signifies a melting transition for the bulk. However, as we shall see, for smaller clusters, this indicator should be taken with some caution. It is useful when examined in conjunction with other indicators such as the specific heat.

We have also calculated the energy deviation,  $\delta E$ ,<sup>23</sup> defined as

$$\delta E = \langle E_{\text{total}}(T) \rangle - [E_0 + (3n - 6) \kappa_B T],$$

where  $\langle E_{\text{total}}(T) \rangle = \langle E_{\text{kin}}(T) \rangle + \langle E_{\text{pot}}(T) \rangle$  is the average total energy of the system at temperature  $T$ , with  $\langle E_{\text{kin}}(T) \rangle$  and  $\langle E_{\text{pot}}(T) \rangle$  being the average kinetic energy and the average potential energy, respectively.  $E_0$  is the ground-state energy and  $(3n - 6) \kappa_B T$  is the vibrational energy in the classical limit.  $\delta E$  may be considered to be an indicator of anharmonicity in the system, as a function of temperature. Following Chuang *et al.*,<sup>23</sup> we smoothed the plots of  $\delta E$  using a three-point moving average method. The error bars in the plot are the standard errors of every three data points.

We also examine carefully the role of simulation time. For this purpose, in Fig. 1 we plot the specific heat for  $\text{Na}_{20}$  with two simulation times: one with 90 ps, and another with 150 ps, per temperature. It may be immediately seen that the 90 ps data result in a premelting feature which is absent for the 150 ps one. This indicates that even for smaller systems such as this, one needs to go to higher simulation times of the order of 150 ps or so.

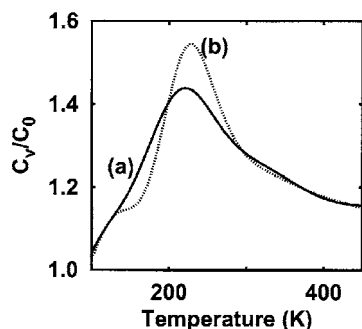


FIG. 1. The specific heat of the  $\text{Na}_{20}$  cluster with simulation time of (a) 150 ps and (b) 90 ps as a function of temperature.

### III. RESULTS AND DISCUSSION

We begin by analyzing the geometries of sodium clusters for the sizes of  $n=8, 10, 13, 15, 20, 25, 40,$  and  $50$ . This is then followed by a discussion on their thermodynamic properties. We also address certain features of  $\text{Na}_{55}$  and  $\text{Na}_{92}$  clusters relevant to the present discussion.<sup>10</sup>

#### A. Geometry

The lowest-energy geometries of sodium clusters are shown in Fig. 2. First, we note that the equilibrium geometries of  $\text{Na}_8, \text{Na}_{13}$  and  $\text{Na}_{20}$ , obtained by us, are in agreement with those reported by R othlisberger *et al.*<sup>24</sup> The ground-state geometry of  $\text{Na}_8$  [Fig. 2(a)] is a dodecahedron. One of its low-energy isomer is an antiprism ( $\Delta E = 0.04$  eV). These two structures play a crucial role in the finite-temperature behavior of this cluster. We find two nearly degenerate structures for  $\text{Na}_{10}$ , namely, a bicapped dodecahedron [Fig. 2(b-i)] and a bicapped antiprism [Fig. 2(b-ii)]. R othlisberger *et al.*<sup>24</sup> have found the bicapped dodecahedron to be unstable. However, we computed the vibrational spectra for both geometries and found the struc-

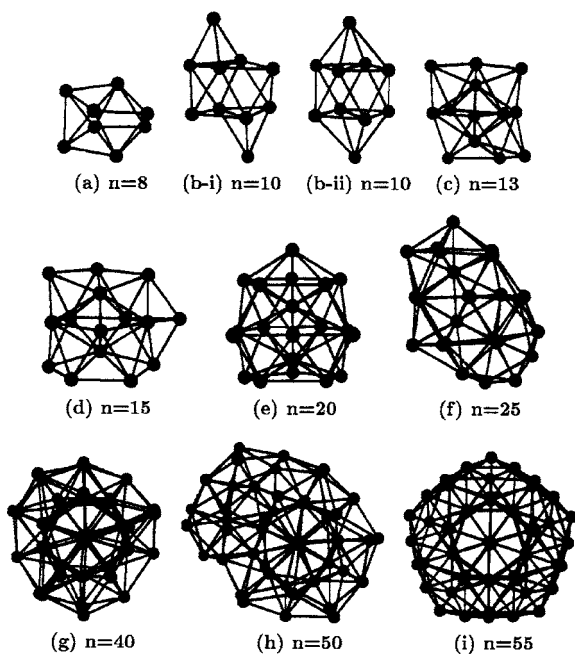


FIG. 2. The ground-state geometries of the  $\text{Na}_n$  ( $n=8-55$ ) clusters.

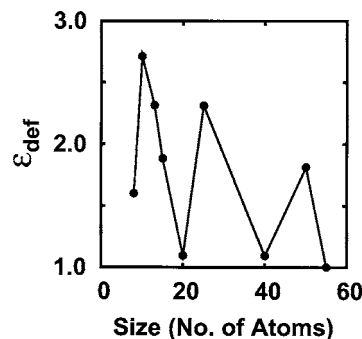


FIG. 3. The deformation parameter  $\epsilon_{\text{def}}$  as a function of size for the ground-state geometries.  $\epsilon_{\text{def}}=1$  indicates a spherical system and  $\epsilon_{\text{def}}>1$  indicates a quadrupole deformation.

tures to be stable. The clusters,  $\text{Na}_{13}$  [Fig. 2(c)] and  $\text{Na}_{15}$  [Fig. 2(d)], exhibit capped pentagonal bipyramidal structures as their lowest-energy configurations. The ground-state geometry of  $\text{Na}_{20}$  [Fig. 2(e)] is a fivefold capped icosahedron, with two atoms capping the icosahedral faces on the central plane. We find a capped double icosahedron to be about 0.11 eV higher in energy than the ground state. The lowest-energy structure of  $\text{Na}_{25}$  has not been previously reported. It may be described as a capped double icosahedron with growth on one side, leading to a distorted nonspherical structure, as shown in Fig. 2(f). The ground-state geometry for  $\text{Na}_{40}$ , shown in Fig. 2(g), agrees with the one reported by Manninen *et al.*<sup>12</sup> It consists of three decahedra capped by the rest of the atoms. The structure is compact and retains the fivefold symmetry. The ground-state geometry of  $\text{Na}_{50}$ , shown in Fig. 2(h), is highly asymmetric. It can be seen from Fig. 2 that a growth towards a 50-at. structure starting from symmetric  $\text{Na}_{40}$  makes the structure nonspherical and asymmetric, which is similar as seen for  $\text{Na}_{25}$  cluster. Finally, the ground-state geometry of  $\text{Na}_{55}$  is a slightly distorted double Mackay icosahedron. It is the most spherical structure and is noted for the sake of completeness.<sup>10</sup>

We also examine the shapes and the eigenvalue spectra of the ground-state geometries of these clusters, as shown in Figs. 3 and 4, respectively. The shape deformation parameter,  $\epsilon_{\text{def}}$  plotted in Fig. 3, for the ground-state geometries of all the clusters show that  $\text{Na}_{20}, \text{Na}_{40},$  and  $\text{Na}_{55}$  are nearly spherical, while  $\text{Na}_{25}$  and  $\text{Na}_{50}$  are deformed. This behavior is also reflected in the eigenvalue spectra of these clusters. The eigenvalue spectra of  $\text{Na}_{20}, \text{Na}_{40},$  and  $\text{Na}_{55}$  clusters (see Fig. 4), having nearly spherical geometries, conform the jellium description. For instance,  $\text{Na}_{55}$  shows a jelliumlike behavior with  $s, p, d, \dots$ , shell structure. However, for systems such as  $\text{Na}_{25}$  and  $\text{Na}_{50}$ , due to the disordered nature of the ground-state geometries, the degeneracy in the eigenvalue spectra is lifted, thereby leading to a continuous spectra.

#### B. Thermodynamics

The thermodynamic behavior is studied by analyzing several indicators. We calculate the specific heat, caloric curve, and Lindemann criterion ( $\delta_{\text{rms}}$ ) as a function of temperature for each cluster. These are shown in Figs. 5–7, re-

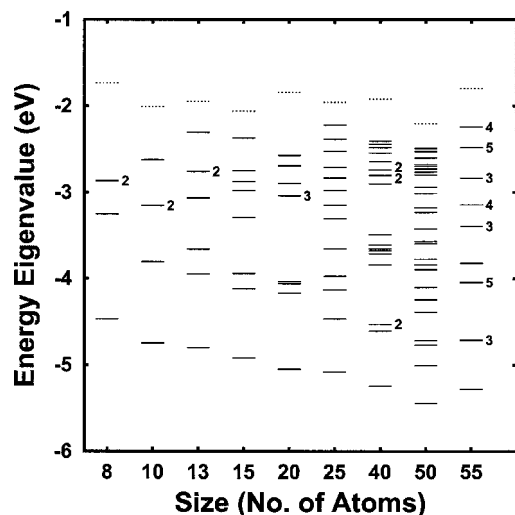


FIG. 4. The eigenvalue spectrum in their ground state as a function of size. The numbers on the right show the degeneracy of that level.

spectively. The melting temperatures,  $T_m$ , taken as the temperature corresponding to the peak in the specific-heat curve, are shown in Fig. 8.

The examination of thermodynamic indicators as a function of cluster size reveals interesting trends. It may be seen that the clusters of sizes 8 and 10 do not show any recognizable peak in the heat capacities. This is also reflected in the caloric curves which increase continuously. While the peak is rather broad for  $n=13-20$ , it progressively becomes narrower as the size increases, and at  $n=92$ , a rather sharp peak with a width of the order of 30 K is observed. The caloric curve (Fig. 6) and the  $\delta_{\text{rms}}$  (Fig. 7) for larger clusters, viz.,  $n=40, 55$ , and 92, clearly show distinct solidlike, liquidlike, and transition regions. Interestingly, the melting temperatures depicted in Fig. 8 show an irregular pattern with the maximum variation of about 60 K. High melting temperatures are observed in two clusters:  $\text{Na}_{40}$  and  $\text{Na}_{55}$ , which are very symmetric;  $\text{Na}_{40}$  exhibiting electronic closure and  $\text{Na}_{55}$  repre-

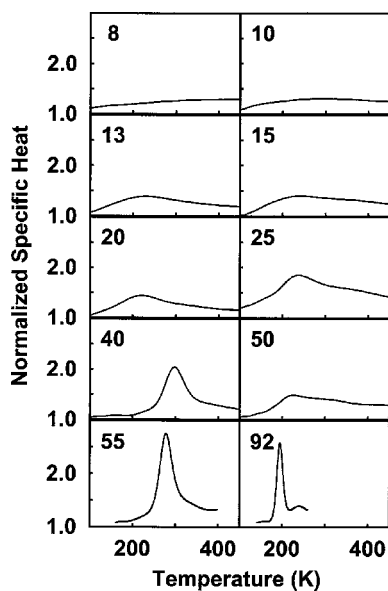


FIG. 5. The normalized specific heat as a function of temperature.

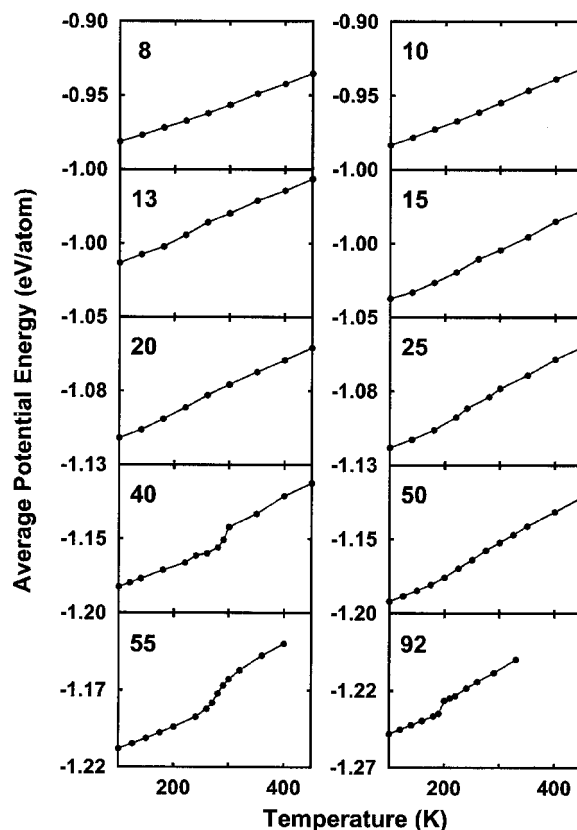


FIG. 6. The averaged potential energy (Caloric curve) as a function of temperature.

sents a geometrically closed system. We plot  $\delta E$  in Fig. 9, which is an indicator of anharmonicity in the system. It is clear from the figure that for the clusters with  $n \geq 40$ , it is possible to distinguish a temperature region ( $< 200$  K) showing harmonic behavior. In contrast to this, the smaller clusters change from harmonic to anharmonic behavior nearly continuously. The most remarkable observation concerns the trends in the specific-heat curve and other indicators for sizes  $n=40, 50$ , and 55. In spite of a well-defined peak in the specific-heat curves for  $\text{Na}_{40}$  and  $\text{Na}_{55}$ , the  $\text{Na}_{50}$  cluster shows a rather broad structure, similar to that seen in smaller clusters. This size-sensitive behavior is discussed further below.

Thus, all the indicators, like the specific heat, the caloric curve,  $\delta_{\text{rms}}$  and  $\delta E$  clearly show that small clusters ( $n=8, 10$ ) do not undergo any meltinglike transition. The examination of their ionic motion indicates that over the entire range of the temperatures the motion is dominated by isomer hopping. This is in agreement with the observation by Rytkönen *et al.*<sup>12</sup> However, these results are in contrast with the SMA and tight binding calculations of Calvo and Spiegelmann,<sup>8</sup> and the Car-Parrinello orbital free calculations of Aguado *et al.*<sup>13</sup> Recall that these calculations, though are not in agreement with each other, show distinct peaks (broader in case of SMA) in the heat capacities of these clusters. Our simulations further show the smaller clusters to be dissociated at about 750 K. Our results for  $\text{Na}_{13}$  and  $\text{Na}_{20}$  are also in disagreement with those by Calvo and Spiegelmann.<sup>8</sup> They calculated the canonical heat capacity of



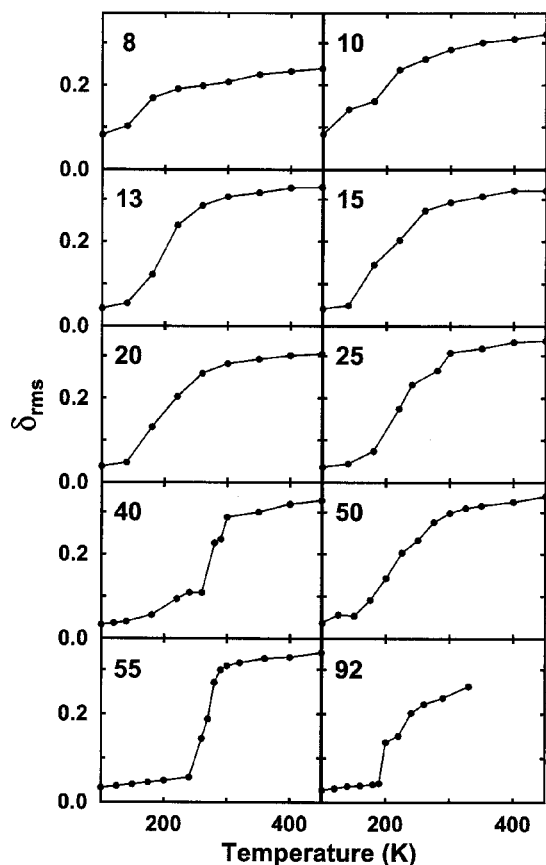


FIG. 7. The root-mean-square bond-length fluctuation  $\delta_{rms}$  as a function of temperature.

$\text{Na}_{13}$ , using an icosahedron for SMA calculations and a pentagonal structure with  $C_1$  symmetry for TB calculations as the ground-state geometries. While the heat capacity with the SMA potential exhibited a single prominent peak, that of TB calculation showed a premelting feature. They attributed this difference to the difference in the ground-state geometries. They further found such premelting feature in the heat capacity of  $\text{Na}_{20}$  cluster, for which they used a capped double icosahedron as the lowest-energy structure. However, our calculations show that this structure is about 0.1 eV higher than the ground-state structure obtained by us for  $\text{Na}_{20}$ . Thus, the differences in the specific heat may be also caused by the differences in the ground-state geometries. The  $\delta_{rms}$  for all the clusters (Fig. 7) clearly shows that for smaller systems

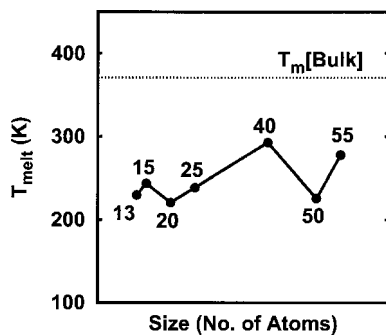


FIG. 8. The melting temperature as a function of size. The melting temperature in bulk ( $T_m[\text{Bulk}]$ ) is 370 K.

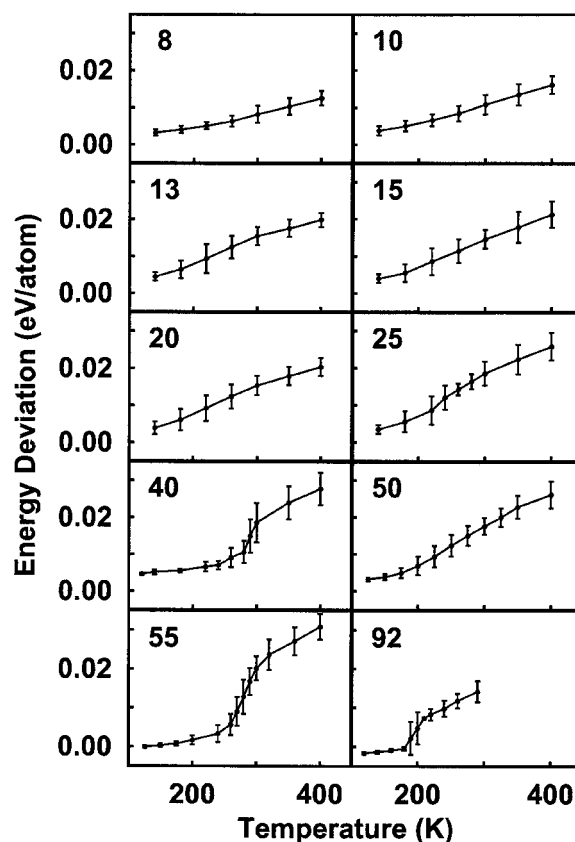


FIG. 9. The deviation of total energy from that of the harmonic limit as a function of temperature. The error bar is the standard error at each temperature.

( $n < 40$ ), it increases almost continuously, whereas for larger ones, a sharp rise is seen that corresponds to the peak in the specific heat. The behavior of  $\delta E$  is, as noted earlier, consistent with this.

Schmidt *et al.*<sup>25</sup> have inferred from their experimental caloric curve that the melting temperature is strongly influenced by the potential-energy contribution. They showed that  $T_m$  follows closely the variation in potential-energy difference between solid and liquid as a function of the cluster size. We have calculated a quantity  $\delta E_{pot}$  defined as the difference of average potential energy of the melted cluster with respect to the ground-state energy. Figure 10 shows the variation of  $\delta E_{pot}$  as a function of size. For this purpose, we have taken the temperatures of liquidlike state as 300 K for  $n=13, 15, 20, 25,$  and  $50$ , and 350 K for  $n=40, 55$ , which are

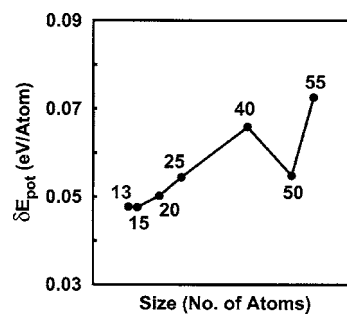


FIG. 10. The potential-energy difference  $\delta E_{pot}$  between ground state and liquidlike state as a function of size.

about 50–70 K higher than the melting temperature of the respective clusters. It can be immediately seen that the variation of  $\delta E_{\text{pot}}$  follows that of the melting temperature (Fig. 8), clearly indicating that the melting temperature is mainly determined by potential-energy contribution. It may be noted that given rather broad nature of melting transition unambiguous estimation of latent heat is very difficult and it is more convenient to examine  $\delta E_{\text{pot}}$  as discussed above.

### C. $\text{Na}_{40}\cdot\text{Na}_{50}\cdot\text{Na}_{55}$

Now, we turn our discussion to the most remarkable observation concerning the trends in the specific heat in going from  $n=40$  to  $n=55$ . As mentioned earlier, while  $\text{Na}_{40}$  and  $\text{Na}_{55}$  show well-defined peaks in the specific-heat curve (peak for  $\text{Na}_{55}$  being much sharper), the peak for  $\text{Na}_{50}$  is rather flat and is almost similar to that of the smaller clusters (say,  $n=13$ – $20$ ). We note that  $\text{Na}_{50}$ , being larger than  $\text{Na}_{40}$ , is expected to show a slightly better melting transition. Interestingly, what is seen is exactly the opposite. It may be noted that such peculiar size sensitivity has been observed experimentally in two systems, namely, clusters of gallium ( $\text{Ga}_n^+$ ,  $n=30$ – $50$  and  $55$ )<sup>6</sup> and clusters of aluminum ( $\text{Al}_n^+$ ,  $n=49$ – $62$ ).<sup>7</sup> For instance, in the case of Ga clusters the heat capacity for  $n=30$  shows a flat curve without a peak. For  $n=31$  it shows a remarkably sharp peak. Interestingly, addition of one more atom (i.e.,  $n=32$ ) diminishes this peak making the heat capacity nearly flat. We believe this behavior to be generic as it has not only been observed experimentally in the case of gallium clusters but also for aluminum cluster and theoretically for sodium clusters in the present simulations.

We note certain peculiar characteristics of the thermodynamic properties of  $\text{Na}_{40}$ ,  $\text{Na}_{50}$ , and  $\text{Na}_{55}$ . We find the melting temperature of  $\text{Na}_{50}$  to be about 60 K lower than that of  $\text{Na}_{40}$  and  $\text{Na}_{55}$ . The  $\delta_{\text{rms}}$  for  $\text{Na}_{50}$  exhibits a gradual increase in the temperature range of 100–300 K. Further, the energy deviation  $\delta E$  for  $\text{Na}_{50}$ , as seen in Fig. 9, starts to increase continuously at about 100 K to up to about 400 K, indicating a continuous change from harmonic behavior to anharmonic one. This behavior of  $\text{Na}_{50}$  is in contrast with that of  $\text{Na}_{40}$  and  $\text{Na}_{55}$ , where the change is seen in a smaller temperature width (of about 30–40 K) around the melting temperature. In order to bring out the origin of this phenomena, we examine the nature of the ground-state geometries for these three clusters.  $\text{Na}_{40}$  and  $\text{Na}_{55}$  are very symmetric structures having

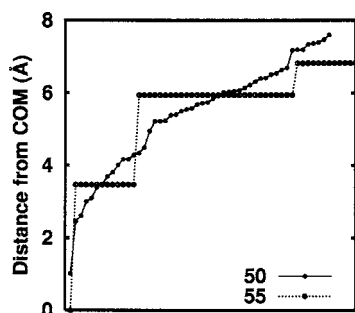


FIG. 11. The distance from the center of mass for the GS geometries of  $\text{Na}_{50}$  and  $\text{Na}_{55}$ .

almost fivefold symmetry. The values of the shape deformation parameter,  $\varepsilon_{\text{def}}$ , shown in Fig. 3, clearly indicate that they are nearly spherical structures. Further, the eigenvalue spectra of the ground-state geometries of  $\text{Na}_{40}$  and  $\text{Na}_{55}$  clusters also show this symmetry, conforming the jellium model. However, the eigenvalue spectrum of  $\text{Na}_{50}$  is very different from those of  $\text{Na}_{40}$  and  $\text{Na}_{55}$ , in the sense that there are levels in the energy gaps leading to a more uniform spectrum. In this sense,  $\text{Na}_{40}$  and  $\text{Na}_{55}$  are ordered, i.e., more symmetric, and  $\text{Na}_{50}$  is amorphous.

In Fig. 11, we show the distances from the center of mass of all the atoms in the ground-state geometries of  $\text{Na}_{50}$  and  $\text{Na}_{55}$ . Clearly, the ordered geometric shell structure of  $\text{Na}_{55}$  is destroyed when five atoms are removed. We believe that the nature of ground-state geometry of the cluster has a significant effect on its melting characteristics. An ordered or symmetric cluster, such as  $\text{Na}_{40}$  and  $\text{Na}_{55}$ , is expected to give rise to a well-defined peak in the heat capacity, while an amorphous and disordered clusters, such as  $\text{Na}_{25}$  and  $\text{Na}_{50}$ , may lead to a continuous melting transition.

### IV. SUMMARY

We have investigated the thermodynamics properties of small sodium clusters,  $\text{Na}_n$ , in the size range of 8–55, using *ab initio* molecular dynamics with simulation time of 1.3–1.8 ns/cluster. We have analyzed several thermodynamic indicators such as the specific heat, caloric curve, Lindemann criterion, and the deviation energy  $\delta E$  to understand the melting characteristics in these clusters. We observe irregular variation in the melting temperatures as a function of size, which has also been seen in the experiments by Haberland and co-workers for larger clusters. The reduction of about 30% than the bulk value in melting temperature of sodium clusters, seen in the experiment is also observed here. Further, we find a strong correlation between the ground-state geometry and the finite temperature characteristics of the sodium clusters. If a cluster has an *ordered* geometry, it is likely to show a relatively sharp melting transition. However, a cluster having a *disordered* geometry is expected to exhibit a broad peak in the specific-heat curve, indicating a poorly defined melting transition. The size sensitivity in the melting transition, seen in experiments by Breaux *et al.*,<sup>6,7</sup> is observed for the case of sodium clusters in the size range of 40 to 50.

### ACKNOWLEDGMENTS

It is a pleasure to acknowledge C-DAC (Pune) for the supercomputing facilities. We also acknowledge partial assistance from the Indo-French Center by providing the computational support. One of us (S.C.) acknowledges financial support from the Center for Modeling and Simulation, University of Pune and the Indo-French Center for Promotion for Advance Research (IFCPAR). We would like to thank Sailaja Krishnamurthy for a number of useful discussions.

<sup>1</sup>M. Schmidt, R. Kusche, B. von Issendorff, and H. Haberland, *Nature* (London) **393**, 238 (1998); M. Schmidt and H. Haberland, *C. R. Phys.* **3**, 327 (2002); H. Haberland, T. Hippler, J. Donges, O. Kostko, M. Schmidt, and B. von Issendorff, *Phys. Rev. Lett.* **94**, 035701 (2005).

- <sup>2</sup>A. A. Shvartsburg and M. F. Jarrold, Phys. Rev. Lett. **85**, 2530 (2000).
- <sup>3</sup>G. A. Breaux, R. C. Benirschke, T. Sugai, B. S. Kinnear, and M. F. Jarrold, Phys. Rev. Lett. **91**, 215508 (2003).
- <sup>4</sup>K. Joshi, D. G. Kanhere, and S. A. Blundell, Phys. Rev. B **66**, 155329 (2002); **67**, 235413 (2003).
- <sup>5</sup>S. Chacko, K. Joshi, D. G. Kanhere, and S. A. Blundell, Phys. Rev. Lett. **92**, 135506 (2004).
- <sup>6</sup>G. A. Breaux, D. A. Hillman, C. M. Neal, R. C. Benirschke, and M. F. Jarrold, J. Am. Chem. Soc. **126**, 8628 (2004).
- <sup>7</sup>G. A. Breaux, C. M. Neal, B. Cao, and M. F. Jarrold, Phys. Rev. Lett. **94**, 173401 (2005).
- <sup>8</sup>F. Calvo and F. Spiegelmann, J. Chem. Phys. **112**, 2888 (2000).
- <sup>9</sup>Y. Li, E. Blaisten-Barojas, and D. A. Papaconstantopoulos, Phys. Rev. B **57**, 15519 (1998).
- <sup>10</sup>S. Chacko, D. G. Kanhere, and S. A. Blundell, Phys. Rev. B **71**, 155407 (2005).
- <sup>11</sup>W. Kohn and L. J. Sham, Phys. Rev. **140**, A1133 (1965).
- <sup>12</sup>A. Rytkönen, H. Häkkinen, and M. Manninen, Phys. Rev. Lett. **80**, 3940 (1998).
- <sup>13</sup>A. Aguado, J. M. López, J. A. Alonso, and M. J. Stott, J. Chem. Phys. **111**, 6026 (1999).
- <sup>14</sup>A. Vichare, D. G. Kanhere, and S. A. Blundell, Phys. Rev. B **64**, 045408 (2001).
- <sup>15</sup>M. C. Payne, M. P. Teter, D. C. Allan, T. A. Arias, and J. D. Joannopoulos, Rev. Mod. Phys. **64**, 1045 (1992).
- <sup>16</sup>D. Vanderbilt, Phys. Rev. B **41**, 7892 (1990).
- <sup>17</sup>Vienna *Ab initio* Simulation Package (VASP), Technische Universität Wien, 1999.
- <sup>18</sup>Z. Li and H. A. Scheraga, Proc. Natl. Acad. Sci. U.S.A. **84**, 6611 (1987); D. J. Wales and J. P. K. Doye, J. Phys. Chem. A **101**, 5111 (1997).
- <sup>19</sup>R. G. Parr and W. Yang, *The Density Functional Theory of Atoms and Molecules* (Oxford University Press, New York, 1989).
- <sup>20</sup>In our earlier work (see Ref. 10), we have verified that an energy cutoff of 3.6 Ry is sufficient. It gives results as accurate as the nearly all-electron projected-augmented wave method (see Ref. 21), taking only  $1s^2$  electrons in the core with an energy cutoff of 51 Ry. The  $\text{Na}_2$  binding energy and bond length by these two methods differ by less than 3%.
- <sup>21</sup>G. Kresse and D. Joubert, Phys. Rev. B **59**, 1758 (1999); P. E. Blöchl, *ibid.* **50**, 17 953 (1994).
- <sup>22</sup>A. M. Ferrenberg and R. H. Swendsen, Phys. Rev. Lett. **61**, 2635 (1988); P. Labastie and R. L. Whetten, *ibid.* **65**, 1567 (1990).
- <sup>23</sup>F.-c. Chuang, C. Z. Wang, S. Ögüt, J. R. Chelikowsky, and K. M. Ho, Phys. Rev. B **69**, 165408 (2004).
- <sup>24</sup>U. Röthlisberger and W. Andreoni, J. Chem. Phys. **94**, 8129 (1991).
- <sup>25</sup>M. Schmidt, J. Donges, Th. Hippler, and H. Haberland, Phys. Rev. Lett. **90**, 103401 (2003).